International Journal of Heat and Technology
Vol. 44, No. 2, April, 2026, pp. 669-678
Journal homepage: http://iieta.org/journals/ijht

Coupled Computational and Experimental Study of Rotary Valve Flow Characteristics and Gifford-McMahon Cryocooler Performance

Debashis Pasa[1], Sachindra Kumar Rout[1*], Shoeb Ahmed Syed[2], Kamala Kanta Muduli[3], Sunil Kumar Sarangi[1], Milon Selvam Dennison[4]

[1] Department of Mechanical Engineering, C. V. Raman Global University, Odisha 752054, India
[2] Dean Faculty of Engineering, Papua New Guinea University of Technology, Lae PMB 411, Papua New Guinea
[3] School of Mechanical Engineering, Papua New Guinea University of Technology, Lae PMB 411, Papua New Guinea
[4] Department of Mechanical Engineering, School of Engineering and Applied Sciences, Kampala International University, Western Campus, Ishaka-Bushenyi P.O Box 71, Uganda

Corresponding Author Email: sachindra106@gmail.com

https://doi.org/10.18280/ijht.440220

Received: 21 November 2025
Revised: 24 March 2026
Accepted: 7 April 2026
Available online: 30 April 2026

Keywords:
Gifford-McMahon cryocooler, Rotary Valve, helium flow path, cryopump, drive mechanism, thermodynamic process

ABSTRACT

The present study is particular about the effect of the flow control valve Rotary Valve (RV), on flow behavior inside the Gifford-McMahon (GM) cold head chamber in proportion to its alternate engagement and disengagement with high-pressure (HP) and low-pressure (LP) flow paths. Cooling is achieved by alternate pressurisation and depressurisation of the cold head chamber along the synchronous movement of the displacer. The performance of the refrigerator is critically linked to that of the RV, particularly to the pressure drop in the valve, which is a function of the rotor position. The passages, by necessity, are narrow and complex in shape. The fluid flow inside the RV has not been explained and investigated properly by past researchers due to the complexity of the valve and the difficulty in understanding it. An attempt has been made to carry out a numerical investigation of an RV inside a GM coldhead, and presented as vectors generated from the numerical simulation, and the flow behavior is presented as a function of the valve rotor position. These results will be useful not only in improving the valve design, but also will contribute to numerical modelling of the complete cryocooler. The Computational Fluid Dynamics (CFD) modelling has been carried out using ANSYS FLUENT software, using inlet and outlet pressure as specified boundary conditions. Overall, this study could provide valuable insights into the fluid flow inside RVs and aid in the design and optimization of cryocoolers.

1. INTRODUCTION

The Gifford-McMahon (GM) cryocooler is employed in a variety of applications, such as cryo-pumping, semiconductor manufacturing, cooling superconducting magnets for MRI machines, and the liquefaction of cryogenic gases like liquid nitrogen and helium. Due to this wide range of applications, numerous research organisations, laboratories, academic institutions, and industries are dedicated to studying and advancing cryocooler technology. The GM cryorefrigerator, developed in the mid-1960s, is engineered to reach cryogenic temperatures, making it suitable for producing liquid nitrogen in a single stage. It offers a variety of production rates depending on the cold head design and dimensions, and it can achieve no-load temperatures below 20 K. These are regenerative types of cryocooler operates at low frequency (2 Hz). A Rotary Valve (RV) inside it is used to control the oscillatory motion of the displacer [1]. The cryocooler uses helium gas as a working fluid. This gas is introduced into and extracted from the system through the RV, which operates in a time-dependent manner to control the high- and low-pressure (LP) cycles. A dedicated compressor unit is utilized to supply and circulate the high-pressure (HP) and the LP gas in the system. The displacer (regenerator) is mainly constituted of stacks of regenerative material, which help to absorb the enthalpy of compressed gas, leading to a decrease in the temperature of the gas. Upon undergoing expansion, the gas experiences a reduction in temperature, leading to the availability of a refrigeration effect at the lower end of the system [2].

2. REVIEW OF LITERATURE

Cryocoolers have been explored through both numerical simulations and experimental studies. The GM cryocooler encompasses a series of thermodynamic processes, including gas compression, gas displacement, heat exchange with a regenerator, and gas expansion [3]. The GM cryocooler is frequently integrated with a cryopump to establish a highly effective vacuum range [4, 5]. Two types of drive mechanisms, namely the scotch yoke and pneumatic drive, are

adopted to achieve synchronization of displacer movement with valve timing and produce a cooling effect in GM cryocoolers. The pneumatic drive mechanism, unlike the scotch yoke drive mechanism, only requires a small amount of HP and LP gas from the compressor to operate, making it a more suitable choice for larger-scale GM cryocoolers [3]. The GM cryocooler is subject to a drawback in the form of high work input per unit of refrigeration, which manifests as losses in the system, such as P-V loss, conduction loss, regenerator thermal loss, and radiation loss. An experimental heat balance analysis was conducted for a single-stage cryocooler, revealing that P-V loss accounted for 82% of the total losses in the system [6]. The dynamic characteristics of a pneumatically driven GM cryorefrigerator were investigated under steady-state conditions. This study used dynamic mathematical modelling to determine variables such as gas masses within the chamber, displacer position, and velocity, taking into account the effects of fluid dynamics and thermodynamics. The model was based on a set of six simultaneous differential equations. Minas [7] conducted a parametric study to investigate the impact of different design parameters on the cooling capacity of a commercially available pneumatically-driven cryorefrigerator. The study was based on the algorithm developed for the dynamic analysis of the GM cryorefrigerator model to conduct the parametric analysis. An optimization design approach was used to determine the optimal values of key design parameters and maximize the cooling performance of the system.

Liu et al. [8] proposed a model to characterize the RV and compressor used in a GM-type pulse tube cryocooler based on SAGE software. The model was validated with experimental results, which included pressure wave, cooling power, and COP. They presented the two major losses due to the inefficient compressor and the RV. RV losses can be divided into two categories: friction and leakage. It was suggested that for a more thorough understanding of the RV operation to avoid having to indirectly determine its characteristics.

Will et al. [9] described two types of valves that have balanced forces on the rotor. In the first valve, the rotor and the stator make no mechanical contact. The second type is a contact valve, like the classical valves, but the forces on the rotor are balanced in a different way. Therefore, these valves are less liable to wear, and the torques needed to rotate the valves are small. They used 'no-contact' valves in four of their systems and discovered that they ran smoothly for two years without any issues. Qiu and Thummes [10] reported a systematic investigation into the effects of valve timing on the cooling performance of a two-stage 4 K pulse tube cooler. Their experiments demonstrate that optimizing valve timing can significantly enhance the cooling performance of both stages.

Further experiments revealed that it was necessary to develop a more efficient RV model. Sumitomo (SHI) Cryogenics of America. Inc has developed a high-capacity, low-noise, single-stage GM cryocooler of the CH series, pneumatically driven CH-160D2 with refrigerating capacity of 525 W/630 W at 77 K at 50 Hz/60 Hz, respectively, designed with a power input of 15–18 kW. They analyzed the performance of the cryocooler at different speed specifications and different regenerators. A performance test was conducted with CH-160D2 by taking two F-70 compressors results cooling capacity of 525 W at 77 K, 50 Hz, at 15 kW-18 kW, with a minimum system temperature of <35 K, whereas by taking one F-100 compressor, the minimum system temperature of <35 K of 11.5 kW–14.5 kW input power [11]. In the case of a dilution refrigerator and quantum computing, a high cooling capacity below 3 K rather than 4.2 K is needed. So, according to the market demand, Cryomech Inc. developed a model PT310 3 K two-stage pulse tube cryocooler with a cooling capacity of 1 W at 3 K on 2nd stage and 35 W at 35 K on the first stage with a power input of 13 kW at 60 Hz. They have analyzed the cooling performance and experimental results of the development [12].

Numerous analyses and adjustments have been carried out to achieve continuous improvements in the cooling performance of the GM cryocooler. This is accomplished through several numerical models, some based on one-dimensional geometry and others on two-dimensional axis-symmetric geometry [13-15]. In addition, several experimental analyses have been conducted to modify the dimensions of the displacer, regenerator, and other components to enhance refrigerating power [16-18]. In a GM cryocooler, the flow control characteristics of the flow control valve are crucial for achieving efficient cooling performance. However, this component has received relatively little attention in research and analysis. So, this flow control valve is basically an RV driven by an externally powered motor or may be an electrically controlled high- and LP solenoid valve. An RV consists of a stator part and a rotor part, and it is rotated on a stator plate surface alternatively to connect with the HP and LP fluid lines. Hence, the fluid flow characteristics of the GM cryocooler can be affected by the waiting time or a change in the angle of opening of the flow path in the RV geometry. In a cycle of operation, there are two short time periods in a coldhead when it is not connected to either the HP side or the LP side (i.e., both valves remain in the closed position). These time periods are known as waiting time periods [19]. So, the flow control characteristics can be availed by changing the waiting period.

If the waiting time period is decreased, the fluid that flows out of the compressor end will have a prolonged contact duration with the expansion chamber of the cold head section. This prolonged contact between the fluid from the compressor end and the expansion chamber of the cold head section increases the flow of acoustic power, leading to an improvement in the cooling capacity. Furthermore, as a result of this, the pressure in both the expansion chamber of the cold head and the HP end of the compressor remains equal for an extended period. This, in turn, causes an increase in the pressure difference between the cold and warm ends of the displacer, while the HP gas in the expansion chamber exerts a greater force to restrict the downward movement of the displacer. Conversely, an increase in the waiting period leads to a decrease in both the pressure difference and the cooling capacity. From a design perspective, it is crucial to determine the optimal waiting period to achieve the minimum pressure difference and maximum refrigeration power. Therefore, an effective flow control mechanism in a GM cryocooler can enhance its cooling performance and minimize the pressure difference between the cold and warm ends of the displacer [20, 21].

The study of valve operation and waiting time in a coldhead part can be studied by both experimental analysis and computational analysis with a real-time simulation tool. By experimental analysis, the result that is achieved may be accurate, but it includes efficient design, fabrication, and manpower, and it is also expensive. Basically, numerical modelling is represented with a set of governing equations

consisting of continuity and momentum equations (representing flow behavior) or may be the energy equation for heat transfer behavior with applicable boundary conditions. So, for analyzing the system performance numerically of the GM cryocooler, several literatures have mentioned the governing equation, as well as their solution methods [13, 22, 23].

Computational Fluid Dynamics (CFD) investigation using ANSYS FLUENT has been utilized by several researchers to investigate various types of valves [24-30]. While there have been numerous studies conducted on the GM coldhead as a whole or on specific components, no previous research has focused on the numerical analysis of the RV in a GM cryocooler. This is primarily due to the complexities involved in the operation and positioning of the valve. Consequently, this study aims to conduct a numerical investigation of the RV in order to examine the fluid flow characteristics inside the cryocooler under varying conditions, such as different valve openings and sizes. The performance of the refrigerator, which is critically linked to that of the RV, particularly to the pressure drop in the valve, is a function of the rotor position. Due to design constraints, the passages are inherently narrow and have a complex shape. The findings are presented in order to demonstrate how the flow behavior varies with changes in the valve rotor position. The outcomes of this study will be beneficial not only for enhancing the design of the valve but also for advancing the numerical modelling of the entire cryocooler system. The CFD modelling has been carried out using ANSYS FLUENT software. The results have been expressed in terms of the flow rate of working fluid under varying high-pressure and HP-LP and cylinder pressure. Till now, very little literature is available on the working analysis of the RV used in the GM cryocooler, and the performance variation of the GM coldhead depending on the compressor frequency [24] has not been studied. So, using CFD, the effect of the RV on GM cryocooler performance is analyzed, and cooling performance studies are done with respect to variable compressor frequencies.

This manuscript is organised into five sections. First, the introduction includes information about the GM cryocooler, its applications, and the importance of the RV in GM-type cryocoolers. Then, the literature gaps and the current motivation of the study. The next section includes a schematic diagram of the GM cryocooler, the structure and geometry of the RV. Next is the methodology (governing equation, boundary conditions, procedure for ANSYS FLUENT simulation) of the current study. Then, the experimental studies of the developed GM cryocooler machine. Following the result and discussion part, and the final section with a conclusion.

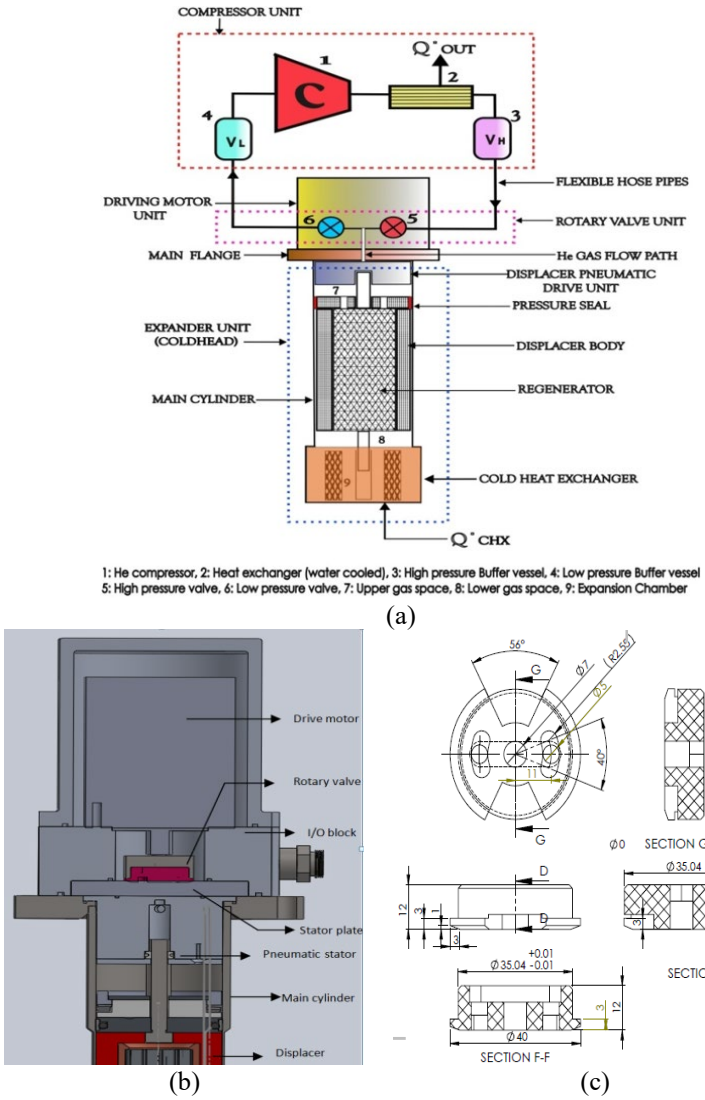

Figure 1. (a) Schematic of Gifford-McMahon (GM) cryocooler unit, (b) physical modelling of the GM cryocooler components, and (c) geometry and dimensions of Rotary Valve (RV) rotor element

3. PROBLEM DESCRIPTION AND MATHEMATICAL FORMULATION

Figure 1(a)–(c) shows a physical model of a single-stage GM cryocooler, which shows the working position of the RV and its link with other components of the coldhead for facilitating the gas flow mechanism in the chamber. The supply of gas flow from the compressor to the cold head and vice versa is controlled by an RV. It consists of a narrow and complex groove flow path (for both HP and LP) for which the displacer up and down motion is synchronized with the RV. The RV gets supply power through a pneumatic drive stator. The RV rotor is a 40 mm diameter component in which the seal element has two wide openings for HP on a line, and perpendicular to it, two other openings for LP are present. The detailed dimension of the RV rotor is mentioned in Figure 1(c). Due to the movement of the motor with the help of an external power supply, the rotor part rotates above the surface of a stator plate, with which it engages alternately with the HP line and LP line. Further, by means of a pneumatic drive, a stator body with HP and LP zones is created above and below the displacer body, which leads to the upward and downward movement of the displacer. For the current study, the working fluid path is the fluid domain that starts from the inlet HP port and ends with the outlet LP port of the coldhead. For the HP line inlet and outlet, the boundaries are the HP port and the expansion chamber of the cold head, respectively (Figures 1–4).

3.1 Boundary conditions and numerical procedure

The fluid flow inside the RV is thought to exhibit the following properties according to the geometry under study: turbulent, three-dimensional, and steady state conditions. As the study is focused to investigate to flow distribution hence energy equation is not used during numerical simulation. The heat transmission fluid is modelled as an incompressible ideal gas with constant physical characteristics across the examined area. As a result, the three-dimensional coordinate system's governing equations are as follows:

Continuity equation of gas flow is:

$$\nabla.\vec{V} = 0 \tag{1}$$

The conservation of momentum equation for gas flow is:

$$\rho((\vec{V}).\nabla)\vec{V} = \rho\vec{g} - \nabla p + \mu(\nabla^2\vec{V}) \tag{2}$$

The presence of wall effects can be analyzed by the help of considering the standard k-ε turbulence model with a set of equations.

For turbulent kinetic energy k:

$$\frac{\partial(\rho k)}{\partial t} + \frac{\partial(\rho k u_i)}{\partial x_i} = \frac{\partial}{\partial x_j}\left[\frac{\mu_t}{\sigma_k}\frac{\partial k}{\partial x_j}\right] + 2\mu_t E_{ij}E_{ij} - \rho\varepsilon \tag{3}$$

For dissipation ε:

$$\frac{\partial(\rho\varepsilon)}{\partial t} + \frac{\partial(\rho\varepsilon u_i)}{\partial x_i} = \frac{\partial}{\partial x_j}\left[\frac{\mu_t}{\sigma_\varepsilon}\frac{\partial \varepsilon}{\partial x_j}\right] + C_{1\varepsilon}\frac{\varepsilon}{k}2\mu_t E_{ij}E_{ij} - C_{2\varepsilon}\rho\frac{\varepsilon^2}{k} \tag{4}$$

where,

u_i: velocity component in respective direction;

E_{ij}: rate of deformation component;

μt: turbulent or eddy viscosity, ($\mu_t = \rho C_\mu \frac{k^2}{\epsilon}$).

Some other model constants with their values are $C_\mu = 0.09$, $\sigma_k = 1.00$, $\sigma_\varepsilon = 1.30$, $C_{1\varepsilon} = 1.44$, $C_{2\varepsilon} = 1.92$.

No-slip boundary criteria are used on the walls of the RV. Numerical modelling has been carried out using ANSYS FLUENT 18.1 with inlet and outlet pressure as specified boundary conditions. The specified values of both pressures are taken from the experimental data conducted in our laboratory, which are (HP = 25 bar, LP = 9 bar). The simulations are conducted for different positions of the RV on the stator plate. By employing suitable boundary conditions to the conservation equations of mass and momentum, and solving using a standard edition of ANSYS FLUENT. K-epsilon turbulent model, pressure-based solver, the second-order upwind used as a numerical scheme for the simulations. The convergence conditions for all equations are set to 10-4. The discretized domain with the nodes of the RV in the computational domain is shown in Figure 4. A non-uniform fine mesh is generated near the valve opening and course mesh is used far away from the valve opening.

3.2 Helium flow path opening under both high-pressure and low-pressure inside the Gifford-McMahon cryocooler with respect to different positions of the Rotary Valve rotor

The fluid flow model with flow direction inside the GM coldhead one is starting from HP port (inlet port) to expansion chamber for incoming fluid path direction, another for returning fluid path direction, i.e., from expansion chamber to LP port (outlet port) has been depicted in Figure 2(a) (for HP flow line) and 2(b) (for LP flow line). When the RV rotor part is rotating on the surface of the stator plate, the openings for fluid flow of these two components overlap with each other and create different cross sections of overlap. The cross-section geometry can be visualized from Figure 3(a) to (d). Figure 3(a)-(d) shows the LP line of flow when the RV rotor is at a specific angle of rotation (θ) proportional to the overlapping percentage of 25, 50, 75,100 respectively, with the RV opening. Figure 4 shows the meshing model for an HP flow path line when the RV opening is with 50% overlapped with the stator plate circular opening path. The represents a discretized domain with nodes of the RV in the computational domain. A non-uniform fine mesh is generated near the valve opening, and course mesh is used far away from the valve opening.

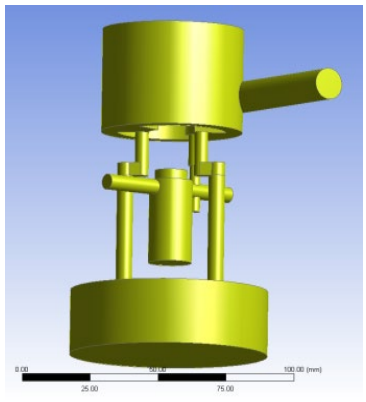

(a)

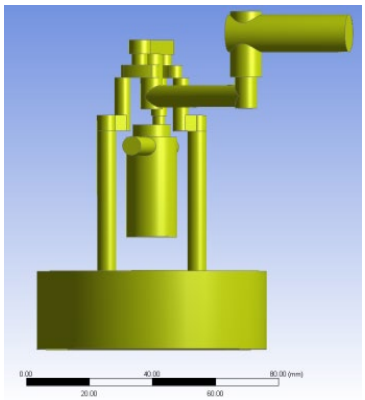

(b)

Figure 2. Fluid flow model of He flow path under (a) high-pressure (HP) and (b) low-pressure (LP) flow line

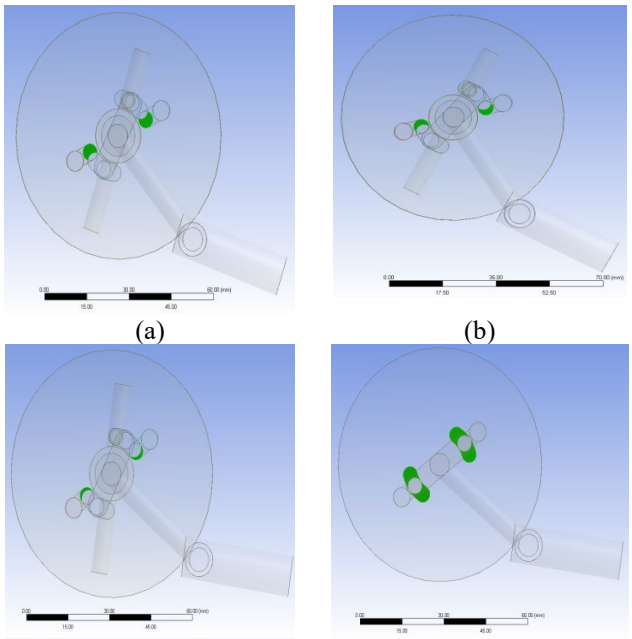

(a) (b)

(c) (d)

Figure 3. Rotary Valve (RV) rotor position at a specific angle of rotation θ for LP line with (a) 25%, (b) 50%, (c) 75%, (d) 100% overlapped with RV opening

3.3 Grid independence test and sensitivity analysis of the mesh

The grid geometry in the computational zone and close to the valve is shown in Figure 4. In addition, the cell size close to the valve opening is kept small to account for the impact of the boundary layer and pressure drop. The fluctuation of the Pressure drop in relation to the quantity of computing cells is shown in the Figure. The Pressure drop value scarcely changes for cell counts more than 375,448, as can be seen, 1,477,012 cells were chosen as the number of cells in the computational zone. Prior to starting the targeted simulations, the grid independence test was performed.

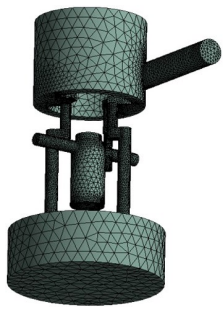

Figure 4. Grid model for a specific high-pressure (HP) flow path

4. OUTCOME AND ANALYSIS

4.1 Pressure and velocity contours

To ensure the precision of the numerical modelling and solver settings utilized in the current study, it is necessary to validate the CFD predicted results by comparing them to experimental data. There is very little literature available that reports the mass flow rate in the valve of a cryocooler. To validate our results, we compared them to the experimental findings of Panda et al. [25] and Xu and Morie [31], who reported a mass flow rate of 4.9 g/s in the valve of the first stage of the cryocooler. The close match between the experimentally measured mass flow rate and the results obtained from the proposed numerical investigation of the RV indicates the high accuracy of the CFD calculations. Once it has been confirmed that the CFD predictions are in close agreement with the experimental results, it is necessary to conduct detailed qualitative and quantitative analyses of the flow behavior and pressure variation at different valve opening positions. This enables the reader to have a better understanding of the complex interaction between the geometry and the flow. The pressure variation contours and velocity vectors resulting from valve opening and closing are presented in Figures 5–7.

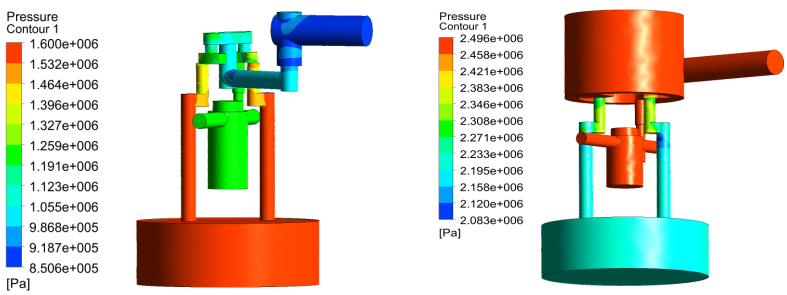

(a) (b)

Figure 5. (a) Pressure contour for low-pressure (LP) flow line and (b) for high-pressure (HP) flow line when 50% overlapping with Rotary Valve (RV) opening

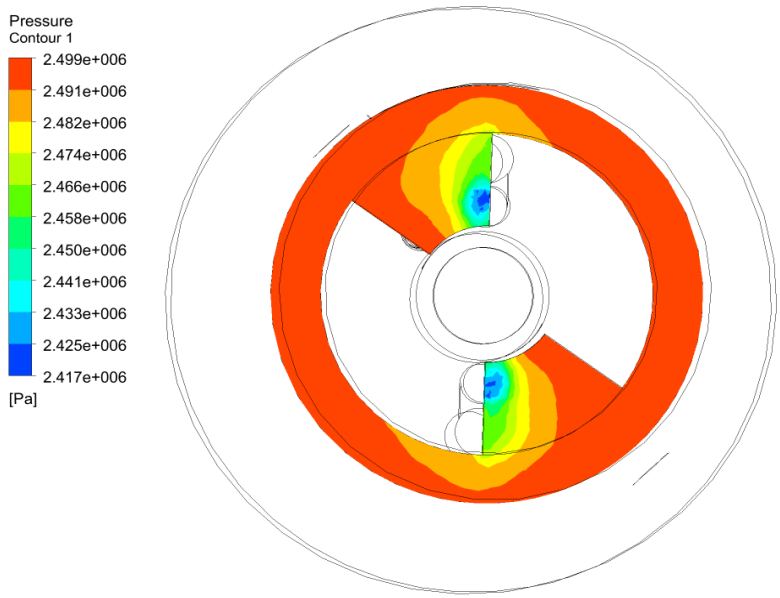

Figure 6. Pressure contour at overlapping of Rotary Valve (RV) opening groove and stator plate opening

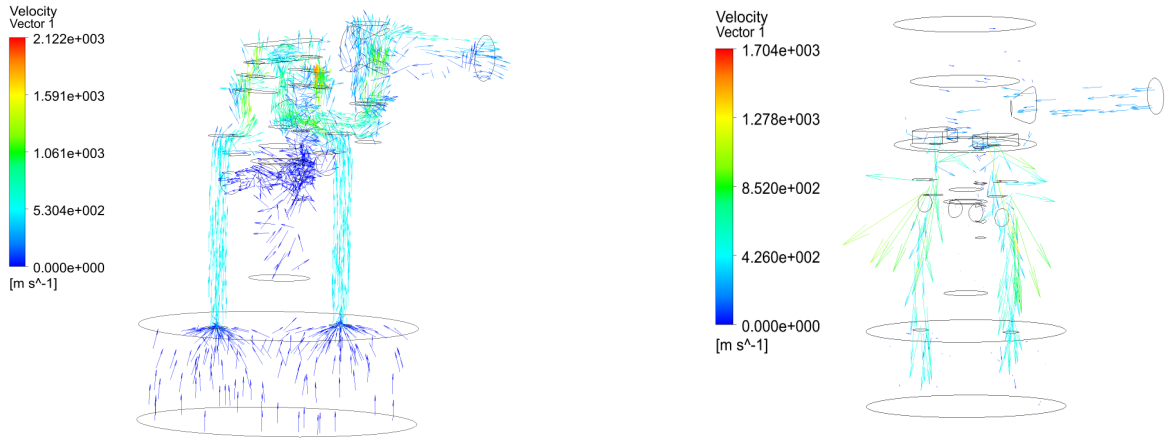

(a) (b)

Figure 7. (a) Velocity vector for low-pressure (LP) flow line and (b) for high-pressure (HP) flow line when 50% overlapping with Rotary Valve (RV) opening

Table 1. Effect of the percentage of overlapping of the Rotary Valve (RV) rotor with the flow opening on different parameters

		For HP Flow Line (HP = 25 bar, LP = 22 bar)				For LP Flow Line (LP = 6 bar, HP = 19 bar)			
Percentage of overlapping (%)		25	50	75	100	25	50	75	100
Θ (degree)		15.8	10.5	5.27	0	16.88	10.86	5.5	0
ṁ (gm/sec)		2.5	4.3	5.3	5.6	3.1	4.7	5.4	5.9
V (m/sec)	in	138.1	233.9	294	306.1	4.59	6.91	7.6	8.7
	out	12.2	26.3	29.1	35.7	186.2	267.4	312.5	351.6

θ: rotation angle of RV rotor, ṁ: mass flow rate, Vin/Vout: inlet/outlet velocity

Note: low-pressure (LP); high-pressure (HP); Rotary Valve (RV).

Table 1 shows the effect of the percentage of overlap of the RV rotor with the flow path opening on different parameters. For high pressure condition (pressure inlet HP = 25 bar and outlet pressure LP = 22 bar) when percentage of overlapping of RV hole with further connection path is 100% means both the paths are coaxial so angle of rotation (θ) is zero which results maximum mass flow rate of 5.6 gm/sec along with maximum velocity values at inlet and outlet likewise when the overlapping percentage decreases the θ value increases and the mass flow rate decreases. Also, it can be visualized for LP conditions.

4.2 Comparison of mass flow rate with respect to different working fluids

The working fluid can be varied for experimental purposes in the GM cryocooler unit. So here, three different working fluids (He, N_2, and air) are taken for a comparative study for

mass flow rate vs. angle of rotation of the RV rotor. Figure 8 for HP flow condition line and Figure 9 for LP flow condition line, which supports the above said comparison study. In both cases, the ṁ values are minimum (5.6 gm/sec at 100% of overlapping in the case of HP condition) at different percentages of opening of RV, i.e., at different angles of rotation of RV rotor for He gas. This can be visualized from the figure. For the other two fluids, i.e., N_2 and air, ṁ values are quite similar for both cases but deviate from the He gas (around 16.1 gm/sec at 100% of overlapping in the case of HP condition and around 16.5 gm/sec for LP condition flow).

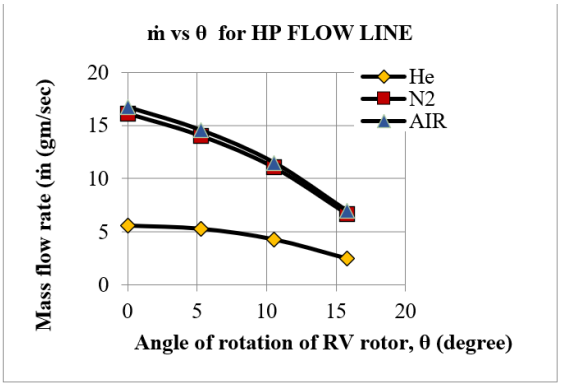

Figure 8. Comparison of mass flow rate with respect to different working fluids for high-pressure (HP) conditions

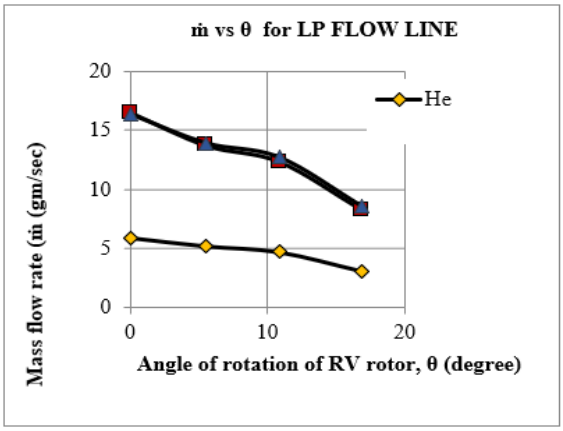

Figure 9. Comparison of mass flow rate with respect to different working fluids for low-pressure (LP) conditions

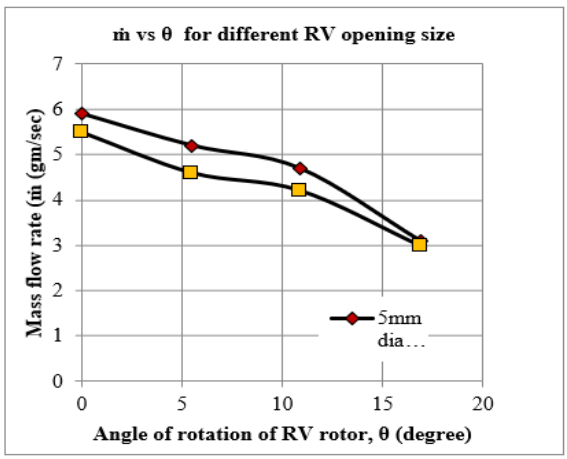

Figure 10. Comparison of mass flow rate with respect to different flow opening paths on the Rotary Valve (RV)

4.3 Comparison of flow rate with respect to different dimensions of Rotary Valve rotor flow path opening

Figure 10 represents the comparison of mass flow rate for two different dimensions of the RV rotor flow path opening for a certain flow condition (here, a LP flow condition is taken for He gas). So, all the above data that are described are for a particular dimension of the RV rotor. In this study, the overall dimension of the rotor is 40 mm in diameter, and its flow opening path is 5 mm in diameter. So, a set of data is found for the mass flow rate by taking the flow opening hole of 4mm in diameter. The figure depicts that there is a variation for both of the cases, and in the case of a 5 mm diameter dimension, ṁ values are maximum (5.9 gm/sec) compared to the lesser dimension (5.49 gm/sec). Accordingly, the velocity value is found to be maximum (8.76 m/sec at the inlet) for a 5 mm dimension for 100% flow opening path, and it is 8.12 m/sec in the case of a lesser dimension opening path.

5. GIFFORD-MCMAHON CRYOREFRIGERATOR TEST RIG

The primary objective of this test rig is to evaluate the performance of the developed GM cryorefrigerator under varying operating conditions. The main elements of the Gifford-McMahon refrigerator (GMR) are shown in Figure 1(a). The helium compressor of the GMR system works in the pressure range of 9–25 bar, depending on load conditions. The compressor generates HP helium gas, and with the help of an RV, the HP and LP sides are connected periodically, resulting in a pressure oscillation for which the displacer moves to and fro inside the main cylinder. The main function of the RV is to disengage the compressor frequency from the GMR frequency. The frequency of the RV for this GM cryorefrigerator is 2 Hz. A buffer vessel (maintained at LP helium gas) is a key component in the whole system for smoothing the pressure and flow during the operation. The main objective of this buffer volume is to sustain the suction pressure for which the scroll of the Helium compressor collects a steady flow of gas regardless of the position of the RV of the coldhead.

HP helium gas passes through a water-cooled heat exchanger, then flows into the regenerator, which is packed with porous material having high heat capacity, high heat transfer area, low pressure drop, and low thermal conductivity (mainly stainless-steel wire mesh of 250 mesh size). The duty of the regenerator is to cool in advance the Helium gas entering the expansion space and reheating the return gas that goes back to the compressor. The cold end heat exchanger (CHX) is the coldest part in the refrigeration system, where the cooling effect is achieved due to the expansion of Helium gas that comes after the regenerator. The schematic of the complete test rig for the GM refrigerator is shown in Figure 11. The cold head part of this system is located inside a vacuum vessel, and the vacuum is maintained using a vacuum pump. Under vacuum conditions, the maximum no-load cooling capacity is achieved as 30 K at the CHX.

6. EXPERIMENTAL SETUP

Experimental analysis has been done to find the cooling performance of the GM coldhead under different pressure

conditions and different compressor frequencies against variable heat load. The cool-down time to achieve liquid nitrogen temperature, i.e., 77 K, is estimated. Also, the optimum compressor frequency is decided after a sufficient time of operation. The coldhead is kept inside a vacuum chamber, and the CHX and main cylinder are covered with multi-layer insulation to minimise the radiation losses during the cooling operation in the vacuum environment. A copper heating plate of the same diameter as the CHX body and 10 mm thick is attached to the CHX bottom face, and 4 numbers of resistance heating elements rated 24 V,50 W are attached to it. By using a voltage regulator, the heat load (0 to 200 W) is provided to the cold end heat exchanger of the GM cold head. The RV is operated by a single-phase 60 rpm AC synchronous motor. The frequency of the RV is 2 Hz. With the help of a Variable Frequency Drive (VFD) supplied with a 3-phase, 50 Hz power supply, the frequency of the scroll compressor is varied from 120 Hz to 200 Hz. Under different compressor frequencies, heat loads are given, and equivalent cooling power is measured using thin-film-based PT 100 temperature sensors. A photograph of the experimental setup of the GM refrigerator is shown in Figure 11.

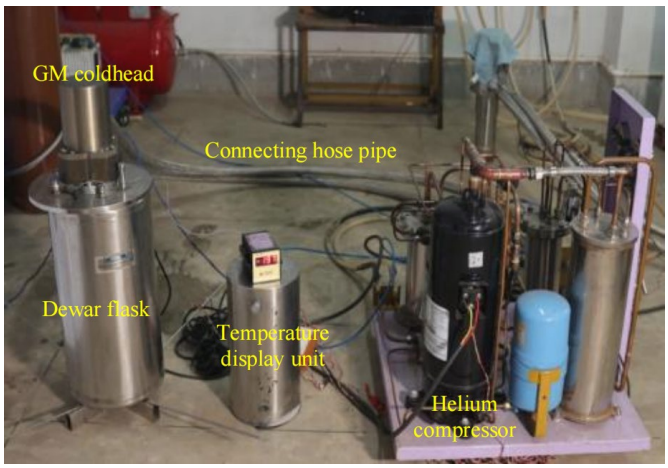

Figure 11. Experimental setup of Gifford-McMahon (GM) cryo refrigerator

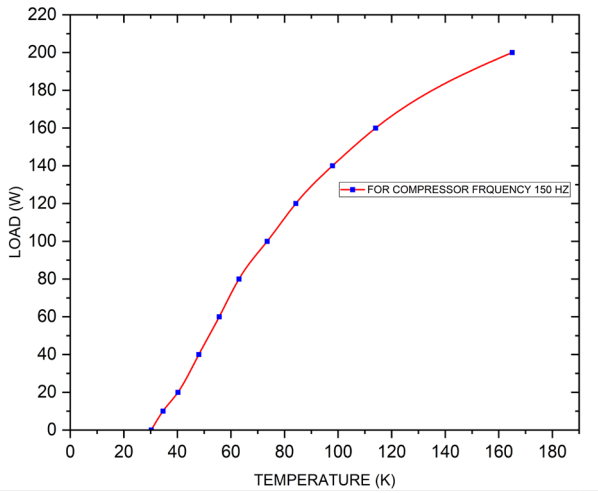

Figure 12. Cooling capacity curve of the Gifford-McMahon (GM) coldhead at a particular compressor frequency

Figure 12 shows the cooling capacity curve for the developed GM refrigerator operated at a compressor frequency of 150 Hz. The net cooling capacity at different temperatures can be visualized from the above plot. Under no load condition the minimum cooling temperature is achieved at 30K at no load. Figure 12 shows the cooling capacity curves under variable compressor frequencies, and the optimum compressor frequency is achieved at 150 Hz, at which the lowest no-load temperature is achieved, i.e., 30 K. Figure 13 illustrates the variation in cooling capacity of the Gifford-McMahon (GM) coldhead under different compressor frequencies.

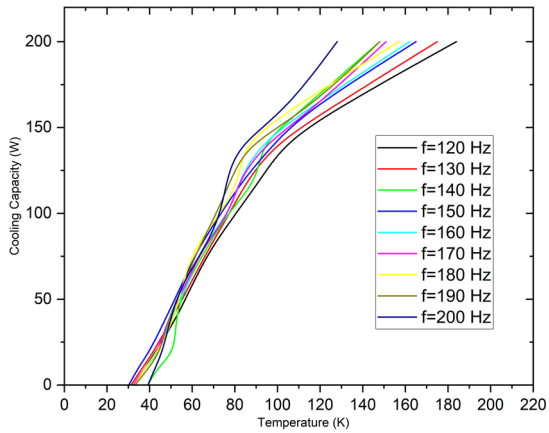

Figure 13. Cooling capacity curve of Gifford-McMahon (GM) coldhead at different compressor frequencies

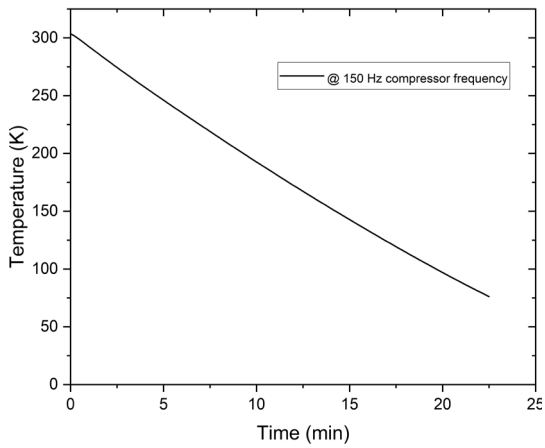

Figure 14. Cool-down curve of Gifford-McMahon (GM) coldhead

The cool-down time of the GM coldhead can be estimated from Figure 14, for attaining the liquefaction temperature of nitrogen gas. It takes 22 min to achieve 77 K at a compressor frequency of 150 Hz.

7. CONCLUSION

The present work is an effort to carry out a numerical simulation analysis (ANSYS FLUENT) of the RV used as a flow control valve in the GM cryorefrigerator using pressure boundary conditions. The simulation results are reasonably consistent with the desired result parameter of the designed cryocooler. The flow friction characteristics of the RV used in the GM cryorefrigerator are analyzed by CFD simulation. The results have been expressed in terms of helium flow rate under

varying HP and LP also in terms of the ṁ vs. θ graph. By changing the angle of rotation value, the percentage of overlapping of RV changes, and for both HP and LP lines, with increasing the overlapping percentage of Helium flow line with narrow opening of component mass flow rate also increases, which can be visualised from the graphs provided. It is observed that the velocity is maximum (8.76 m/sec at the inlet) for a 5 mm dimension for 100% flow path opening, and it is 8.12 m/sec in the case of a lesser dimension opening path. A comparison study of the mass flow rate has also been performed by taking three different working fluids used in the cryocooler unit, and the result found is satisfactory as per the result parameter of the concerned cryocoolers. The study also gives a direction for a two-stage cryocooler, both numerically and experimentally.

ACKNOWLEDGMENT

This work has been supported by the Board of Research in Nuclear Science (BRNS) under grant No.: 59/14/03/2021-BRNS/57032. The authors are also grateful to Dr. Debakant Samal, Institute of Physics, Bhubaneswar, for our Principal collaborator for his continuous academic and technical support.

REFERENCES

[1] Radebaugh, R. (2009). Cryocoolers: The state of the art and recent developments. Journal of Physics: Condensed Matter, 21(16): 164219. https://doi.org/10.1088/0953-8984/21/16/164219

[2] Huang, B.J., Chang, S.C. (1995). System performance analysis of Gifford-McMahon cooler. Cryogenics, 35(2): 117-125. https://doi.org/10.1016/0011-2275(95)92880-2

[3] Lei, T., Zuev, Y.L., Bao, Q., Xu, M. (2020). Drive force optimization of a pneumatically-driven Gifford-McMahon cryocooler by numerical modeling. IOP Conference Series: Materials Science and Engineering, 755(1): 012048. https://doi.org/10.1088/1757-899X/755/1/012048

[4] Iwasa, Y., Ito, S. (1996). A new type of cryopump with a metal cryopanel cooled below 3.6 K by a two-stage GM refrigerator. Vacuum, 47(6-8): 675-678. https://doi.org/10.1016/0042-207X(96)00044-9

[5] Meng, D., Sun, L., Yan, R., Shao, R., et al. (2017). Effects of cryopump on vacuum helium leak detection system. Vacuum, 143: 316-319. https://doi.org/10.1016/j.vacuum.2017.06.036

[6] Thirumaleshwar, M., Subramanyam, S.V. (1986). Heat balance analysis of single stage Gifford-McMahon cycle cryorefrigerator. Cryogenics, 26(3): 189-195. https://doi.org/10.1016/0011-2275%2886%2990218-3

[7] Minas, C. (1992). Parametric analysis and optimization of a Gifford-McMahon cryorefrigerator. Cryogenics, 32(12): 1125-1130. https://doi.org/10.1016/0011-2275(92)90326-6

[8] Liu, D., Dietrich, M., Thummes, G., Gan, Z. (2017). Numerical simulation of a GM-type pulse tube cryocooler system: Part II. RV and cold head. Cryogenics, 81: 100-106. https://doi.org/10.1016/j.cryogenics.2016.11.006

[9] Will, M.E., Tanaeva, I.A., Li, R., De Waele, A.T.A.M. (2004). New RVs for pulse-tube refrigerators. Cryogenics, 44(11): 793-800. https://doi.org/10.1016/j.cryogenics.2004.03.022

[10] Qiu, L.M., Thummes, G. (2002). Valve timing effect on the cooling performance of a 4 K pulse tube cooler. Cryogenics, 42(5): 327-333. https://doi.org/10.1016/S0011-2275(02)00043-7

[11] Gandla, S.K., Xu, M., Dunn, S. (2023). Development of a high capacity single stage GM cryocooler at 30 K range. Cryogenics, 132: 103664. https://doi.org/10.1016/j.cryogenics.2023.103664

[12] Hao, X., Cosco, J., Dausman, R. (2022). Development of high cooling capacity 3 K two stage pulse tube cryocooler. Cryocoolers, 22: 227-233.

[13] Xu, M., Morie, T. (2014). Numerical simulation of the second stage regenerator in a 4 K GM cryocooler. AIP Conference Proceedings, 1573(1): 1143-1148. https://doi.org/10.1063/1.4860834

[14] Wang, C. (1997). Numerical analysis of 4 K pulse tube coolers: Part II. Performances and internal processes. Cryogenics, 37(4): 215-220. https://doi.org/10.1016/S0011-2275%2897%2900014-3

[15] Zhi, X., Pfotenhauer, J.M., Miller, F., Gershtein, V. (2017). Numerical study on the working performance of a GM cryocooler with a mechanically driven displacer. International Journal of Heat and Mass Transfer, 115: 611-618. https://doi.org/10.1016/j.ijheatmasstransfer.2017.07.058

[16] Xu, M.Y., Morie, T., Tsuchiya, A. (2017). Development of tin-plated regenerator material. IOP Conference Series: Materials Science and Engineering, 171(1): 012076. https://doi.org/10.1088/1757-899X/171/1/012076

[17] Xu, M.Y., Morie, T., Tsuchiya, A. (2017). Development of zinc-plated regenerator material. IOP Conference Series: Materials Science and Engineering, 278(1): 012167. https://doi.org/10.1088/1757-899X/278/1/012167

[18] Li, X., Xu, D., Shen, F.Z., Liu, H.M., Li, L.F. (2019). Design of a multi-layer insulation (MLI) measurement system with a GM cryocooler. IOP Conference Series: Materials Science and Engineering, 502(1): 012075. https://doi.org/10.1088/1757-899X/502/1/012075

[19] Zhu, S., Kakimi, Y., Matsubara, Y. (1998). Waiting time effect of a GM type orifice pulse tube refrigerator. Cryogenics, 38(6): 619-624. https://doi.org/10.1016/S0011-2275(98)00026-5

[20] Xu, M., Gao, J.L. (2014). U.S. Patent No. 8,783,045. Washington, DC: U.S. Patent and Trademark Office.

[21] Xu, M., Gao, J.L., Seitz, E., Saito, M. (2010). U.S. Patent No. 7,654,096. Washington, DC: U.S. Patent and Trademark Office.

[22] Bao, Q., Xu, M.Y., Tsuchiya, A., Li, R. (2015). Recent development status of compact 2 K GM cryocoolers. IOP Conference Series: Materials Science and Engineering, 101(1): 012136. https://doi.org/10.1088/1757-899X/101/1/012136

[23] Wang, C., Hanrahan, T., Cosco, J. (2018). A large single-stage GM cryocooler for operating temperatures of 13-30K. In Proceedings of 20th International Cryocooler Conference, Burlington Vermont.

[24] Khute, S., Pasa, D., Pulagam, M.K.R., Rout, S.K., Sarangi, S.K. (2023). A systematically organized series of mathematical calculations for the development of a

helium compressor tailored for a Gifford–McMahon cryocooler. In Conference on Fluid Mechanics and Fluid Power, Springer Nature Singapore, Singapore, pp. 675-689. https://doi.org/10.1007/978-981-97-7388-6_55.
[25] Panda, D., Sarangi, S.K., Satapathy, A.K. (2019). Influence of characteristics of flow control valves on the cooling performance of a GM cryocooler. Vacuum, 168: 108836. https://doi.org/10.1016/j.vacuum.2019.108836
[26] Wu, D., Li, S., Wu, P. (2015). CFD simulation of flow-pressure characteristics of a pressure control valve for automotive fuel supply system. Energy Conversion and Management, 101: 658-665. https://doi.org/10.1016/j.enconman.2015.06.025
[27] Qian, J.Y., Wei, L., Jin, Z.J., Wang, J.K., Zhang, H., Lu, A.L. (2014). CFD analysis on the dynamic flow characteristics of the pilot-control globe valve. Energy Conversion and Management, 87: 220-226. https://doi.org/10.1016/j.enconman.2014.07.018
[28] Lisowski, E., Czyżycki, W., Rajda, J. (2013). Three dimensional CFD analysis and experimental test of flow force acting on the spool of solenoid operated directional control valve. Energy Conversion and Management, 70: 220-229. https://doi.org/10.1016/j.enconman.2013.02.016
[29] Lisowski, E., Rajda, J. (2013). CFD analysis of pressure loss during flow by hydraulic directional control valve constructed from logic valves. Energy Conversion and Management, 65: 285-291. https://doi.org/10.1016/j.enconman.2012.08.015
[30] Aung, N.Z., Yang, Q., Chen, M., Li, S. (2014). CFD analysis of flow forces and energy loss characteristics in a flapper–nozzle pilot valve with different null clearances. Energy Conversion and Management, 83: 284-295. https://doi.org/10.1016/j.enconman.2014.03.076
[31] Xu, M., Morie, T. (2012). Numerical simulation of 4K GM cryocooler. Cryocoolers, 17: 253-259.